Smart Lighting Systems as a Demand Response Solution for Future Smart Grids

Chi Kwan Lee, *Senior Member, IEEE*, Heng Liu, Desiree Fuhs, André Kores, and Eberhard Waffenschmidt, *Senior Member, IEEE*

***Abstract*— Massive deployment of distributed and intermittent renewable energy sources cause instability in the power system because of the mismatch between the power generation and load consumption. In order to solve this problem, smart loads embedded with modern power electronic converters and communication devices are being developed. They are able to communicate with the utility and perform automatic demand response. In this paper, we propose a smart light-emitting diode (LED) driver for lighting. This smart LED driver adjusts its electricity usage in response to the utility without the expense of human visual comfort. To achieve this goal, a new control method is developed and a typical rate of change of LED power is determined through conducting a series of visual assessments with interviewees. An experimental smart LED driver is built to validate the new control method. Experimental report from the visual assessments has confirmed that the proposed control method can significantly reduce the light flickering caused by the change of LED power.**

***Index Terms*— Demand response, renewable energy, smart grid, smart lighting.**

I. Introduction

CLIMATE and energy issues have greatly prompted the development of renewable energy sources worldwide in the past few decades. Many countries have set the target to achieve 20% of renewable energy sources to replace conventional fossil fuels in electricity generation by 2020 [1], [2]. Among the renewable energy sources, wind and solar are the two most popular technologies [3]. Taking advantages of their ubiquity and abundance, they have gained widespread utilization at different scales and capacity levels ranging from large wind/solar farms to small rooftop wind turbine or solar panel. Different from the traditional power generation, wind and solar are intermittent, which leads to grid stability problems such as voltage fluctuation and frequency deviation with their massive integration into power grid [4]. State-of-the-art active and reactive power compensators such as static synchronous compensator [5], [6] and battery energy storage system [7], [8] were developed to enhance the voltage and frequency regulations. At present, end-use customers have participated in the operation of the electric grid through the demand response [9] to improve the power system stability and reliability. On the demand side management, classical measurement, including time of use tariffs, direct load control, and real-time pricing [10], [11] are used to encourage end-use customers to change their electricity consumption to follow the power generation. Smart loads embedded with modern power electronic converters are able to continuously control the load power effectively. The concept of smart appliances [12]–[14], such as water heaters [15], ice-thermal storage system [16], passive LED lighting system [17], [18], and plug-in electric vehicles [19], have been demonstrated. Moreover, modern information and communication technology (ICT) [20], [21] also facilitates smart appliances to adapt their energy consumption to electric utility.

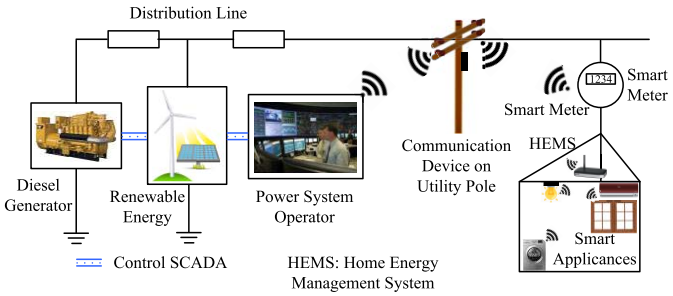

Fig. 1. Future smart grid and smart home.

As shown in Fig. 1, the home energy management system (HEMS) gathers the information and power consumption of each electric appliance. The aggregate power demand and operating reserve are reported to the utility through the smart meter. The utility may signal demand requests to the customers by price incentives. Customer could manage their appliances in response to the demand requests by setting up the conditions in the HEMS, such as price threshold, priorities, maximum/minimum power of the appliance, and so on. Through receiving power commands from the HEMS, the smart controllers installed in the electric appliances are able to estimate the load states and control their power consumption. As a result, the mismatching between the demand and supply can be diminished.

In view of great lighting demand in residential, commercial, and industrial buildings [22], lighting devices are promising

Manuscript received August 22, 2018; revised November 15, 2018; accepted December 8, 2018. Date of publication January 1, 2019; date of current version August 4, 2020. This work was supported in part by the Research Grant Council of Hong Kong through Germany/Hong Kong Joint Research Scheme under Grant G-HKU701/15, in part by Theme-Based Research Scheme under Grant T23-701/14-N, and in part by Deutsche Akademische Austauschdienst (DAAD) e.V., PPP Hongkong, Projekt-ID 57216001. Recommended for publication by Associate Editor J. Marcos Alonso. *(Corresponding author: Chi Kwan Lee.)*

C. K. Lee and H. Liu are with CIRE-Cologne Institute for Renewable Energy, TH Kölnâ University of Applied Sciences, 50678 Cologne, Germany (e-mail: desi.fuhs@googlemail.com; andre.kores@gmx.de; eberhard.waffenschmidi@th-koeln.de).

D. Fuhs, A. Kores, and E. Waffenschmidt are with the Cologne University of Applied Sciences, 50678 Cologne, Germany (e-mail: desi.fuhs@googlemail.com; andre.kores@gmx.de; eberhard.waffenschmidi@fh-koeln.de).

Color versions of one or more of the figures in this article are available online at http://ieeexplore.ieee.org.

Digital Object Identifier 10.1109/JESTPE.2018.2890385

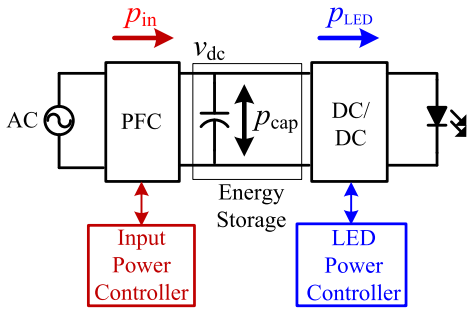

Fig. 2. Block diagram of a smart LED driver.

candidates for future smart loads. In this paper, an LED driver is transformed into a smart lighting device that can adapt its power consumption without intrusive impact to the users. A new control method is developed to coordinate the input ac power and LED power. The rest of this paper is organized as follows. Topology and control method of the proposed smart LED driver is first introduced in Section II. The details of how to determine the maximum rate of change of LED power through a series of visual assessments are described in Section III. The design of the power electronics circuits and control implementation of the smart LED driver are presented in Section IV. The experimental results are reported in Section V. Section VI concludes this paper.

II. Smart LED Driver

A. Topology and Control Method

Fig. 2 shows the block diagram of the proposed smart LED driver which is a classical two-stage power converter. The first stage is a power factor correction (PFC) converter shaping the input ac current into sinusoidal and in-phase with the ac voltage. The second stage is a dc/dc converter controlling the LED power. Under normal situation, the power of LED lamp is regulated by the smart LED driver at a preset value or following the dimming command from the user. When excess renewable energy is fed into power grid, the smart LED driver will be instructed by power system operator (via ICT) to increase its power consumption. The smart LED driver will also be instructed to perform load shedding when there is a drop of renewable energy generation. Electrolytic dc capacitors are connected at the output of PFC converter to filter the ac ripple and provide a constant dc voltage for the second-stage dc/dc converter. The power flow directions inside the proposed smart LED driver are also illustrated in Fig. 2.

In this paper, an unconventional control method using input-feed forward control is proposed. The input power p_{in} is directly controlled by the PFC converter to follow the power command from the power system operator or user. Thus, the dc-link capacitor voltage v_{dc} is not tightly regulated at a constant value. v_{dc} is allowed to vary between the maximum and minimum voltage limits. The variation of v_{dc} is fed to the second-stage dc/dc converter to control the power of LED. However, the rate of change of LED power will be controlled in order to provide good visual comfort for the user. Two timing diagrams are depicted in Fig. 3 showing the change of input ac power p_{in} and power of LED p_{LED},

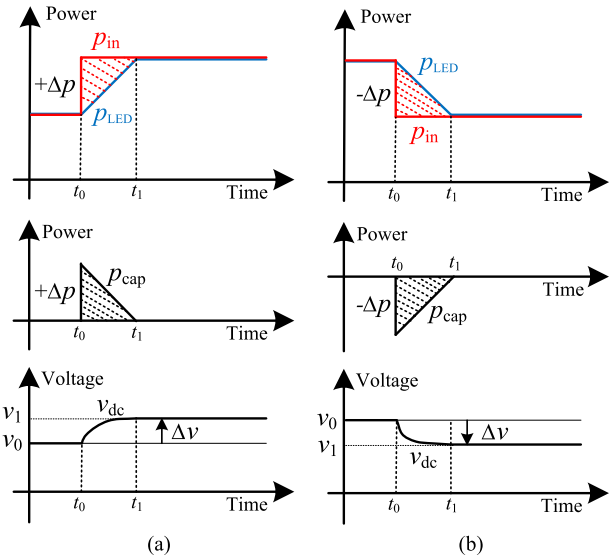

Fig. 3. Timing diagrams showing the operations of the proposed smart LED driver. (a) Increasing power consumption. (b) Decreasing power consumption.

power absorbed/delivered by the dc-link capacitor p_{cap}, and voltage across the dc-link capacitor v_{dc}.

In Fig. 3(a), the smart LED driver receives the command from the power system operator at t_0 to temporarily increase its power consumption by Δp. The input power controller generates the control command $(p_{in}+\Delta p)$ immediately. Since the maximum rate of change of p_{LED} is controlled by the second-stage dc/dc converter, the excess power $+\Delta p$ will be absorbed by the dc-link capacitor. Hence, v_{dc} increases. From t_0 to t_1, the second-stage dc/dc converter is prompted by the rise of v_{dc} to increase the LED power progressively until it is equal to p_{in}. At t_1, v_{dc} reaches a new steady-state value. In Fig. 3(b), the power system operator responds to a sudden drop of renewable energy generation and sends command to the smart LED driver to decrease the LED power by $-\Delta p$ as shown in Fig. 3(b). p_{LED} reduces gradually until it matches the new p_{in} with a new dc voltage. The difference in energy consumption between t_0 and t_1 is supplemented by the dc-link capacitor. Note that p_{LED} does not follow p_{in} instantaneously because rapid change of LED power leads to a significant change of LED brightness causing intrusive lighting to users. The determination of a typical rate of change of LED power is closely related to the sensitivity of the human eye to light of a certain intensity which will be discussed in Section III.

B. Maximum and Minimum Voltage of the DC-Link Capacitor

The dc-link capacitor is an energy buffer between the PFC and dc/dc converters to temporarily absorb or deliver energy from the ac input or to the dc output. Therefore, the voltage variation across the capacitor is determined by not only the amplitude but also the duration of the power difference between the ac input and dc output. Ignoring the power loss of the converters, the input power can be represented as

$$p_{in} = p_{cap} + p_{LED} \tag{1}$$

where p_{in}, p_{LED}, and p_{cap} are input power, LED power, and power of the dc-link capacitor, respectively. It is assumed that there is a step input power change Δp at t_0 and p_{LED} changes linearly with time until it reaches p_{in} at t_1. During $t_0 - t_1$, the mathematical relationship can be formulated by integrating (1). Then, we have

$$\int_{t_0}^{t_1} p_{\text{in}} \mathrm{d}t = \int_{t_0}^{t_1} p_{\text{cap}} \mathrm{d}t + \int_{t_0}^{t_1} p_{\text{LED}} \mathrm{d}t \tag{2}$$

and

$$t_1 - t_0 = \frac{\Delta p}{\text{RoC}} \tag{3}$$

where RoC is the rate of change of LED power. Larger the value of RoC is, more rapidly the LED power changes. Substituting (3) into (2) gets

$$\frac{\Delta p^2}{\text{RoC}} = \Delta E_{\text{cap}} + 0.5 \frac{\Delta p^2}{\text{RoC}} \tag{4}$$

where ΔE_{cap} is the energy buffered by the dc-link capacitor. It can be rewritten by the relation between the voltage and size of the capacitor and expressed as

$$\Delta E_{\text{cap}} = 0.5C\left(v_1^2 - v_0^2\right) \tag{5}$$

where C is the capacitance, v_0 and v_1 are the voltages of the dc-link capacitor at t_0 and t_1, respectively. Substituting (5) into (4) gets

$$\frac{\Delta p^2}{\text{RoC}} = C \times \left(v_1^2 - v_0^2\right). \tag{6}$$

The input power change Δp can be expressed as

$$\Delta p = \sqrt{\text{RoC} \times C \times \left(v_1^2 - v_0^2\right)} \tag{7}$$

and the corresponding voltage variation Δv across the dc-link capacitor can be obtained as

$$\Delta v = \sqrt{\frac{\Delta p^2}{\text{RoC} \times C} + v_0^2} - v_0. \tag{8}$$

III. Human Eye Response to Light Intensity

The rate of change of LED power should be limited in order to ensure the visual comfort. The brightness of an LED increases when the power increases. However, the human eye does not perceive the same actual light. The difference between actual and perceived light levels results from physiological factors such as pupil dilation, eye saturation, adaption, and other human and environmental factors. Studies have shown that our eye perceives light in a logarithmic manner as illustrated in Fig. 4 [23]. It can be approximately represented by a squared power relationship with the actual light. The perceived light can be expressed as

$$\text{Perceived light} = \sqrt{\text{Actual light}}. \tag{9}$$

Our eye perceives more than the actual light. For an example, a light source dimed to 50%, we perceive about 70% of the original light level. Taking the derivative of perceived light with respect to actual light obtains

$$\frac{d(\text{Perceivedlight})}{d(\text{Actual light})} = \frac{0.5}{\sqrt{\text{Actual light}}}. \tag{10}$$

It is important to note that the variation of light intensity is much easier to be noticed by the human eye in low light level than high light level. We are not very susceptible to the change of light intensity in a bright environment.

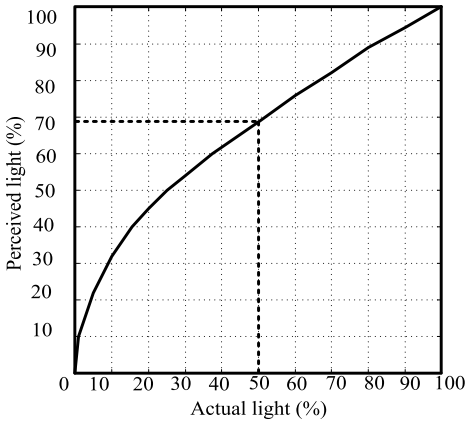

Fig. 4. Comparison of perceived and actual light level.

TABLE I
LED Lamp and Driver Specifications

Room	*1.8m × 1.7m × 2.2m*
LED	*Philips Fortimo LED DLM Module 2000 32W/840*
Electronic driver	*TI UCC28810EVM-002*

To experimentally determine a typical rate of change of LED power at different power levels, a survey is conducted in a light chamber to find out how people tolerate the change of light intensity. Fig. 5 illustrates the dimensions and setup of the light chamber. An LED lamp with electronic driver is installed in the middle of the ceiling. The specifications of the LED lamp and driver are shown in Table I. A 32-W LED is used to provide the illumination level around 500 lux, which is recommended for normal working places according to the international standards [25], [26]. The test begins with an initial LED current $I_{\text{LED}}(0)$ and rate of change of LED current which is represented with a specific current step ΔI at the time step Δt. The LED current $I_{\text{LED}}(n)$ increases progressively with time $t(n)$ until it reaches rated current of the LED. Interviewees sitting in the light chamber are required to fill out a questionnaire to rate how they observe the change of light intensity over time. The scale ranges from 1 (not noticeable) to 10 (very obvious). The average value of interviewees' scores is used to modify the rate of change of LED current. The rate of change of LED current will be increased if the average score is below the desired value. Conversely, it will be decreased. The test will be repeated with a new rate of change of LED current until the majority of the interviewees do not notice the light variation. Fig. 6 shows the flowchart of the test in an iterative approach. The test has been carried out at different LED currents.

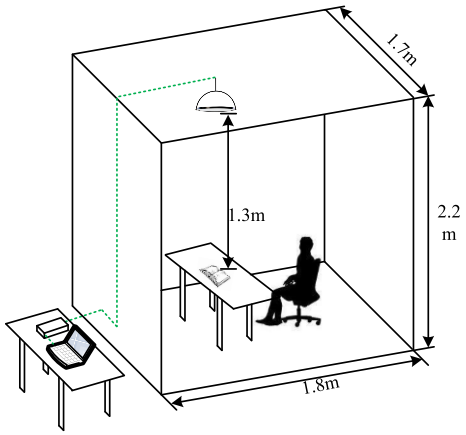

(a)

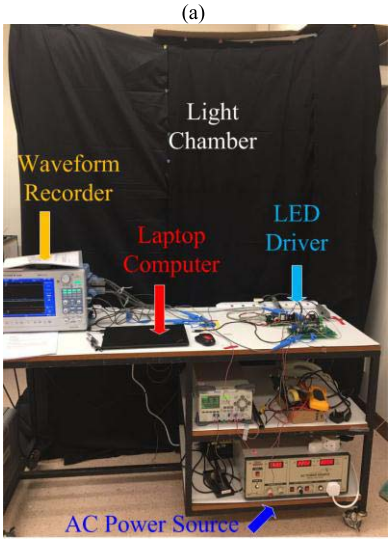

(b)

Fig. 5. (a) Dimension of the light chamber. (b) Photograph of the setup.

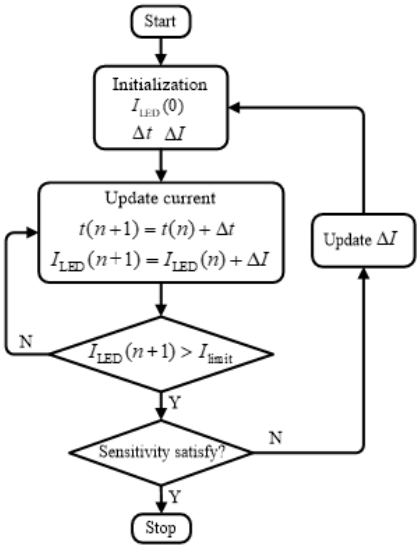

Fig. 6. Flowchart of human eye response to light intensity test.

The details of the survey are presented in [24]. The most important results of the survey are summarized in the Appendix. According to the data collected in the survey,

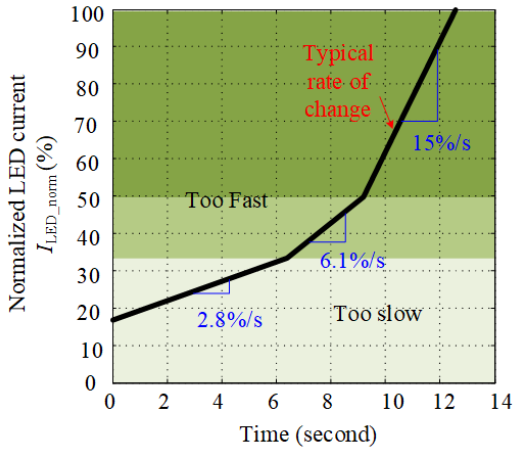

(a)

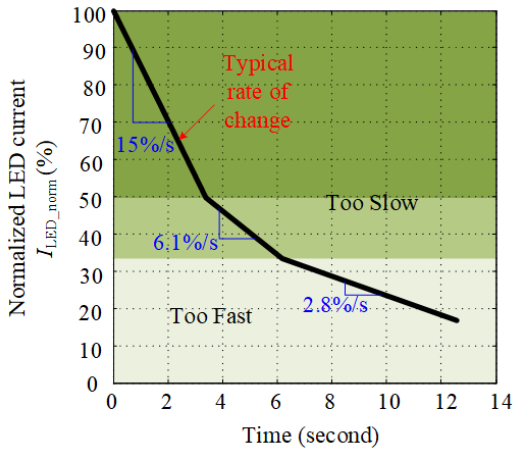

(b)

Fig. 7. Normalized typical rate of change of LED current from 15% to 100% of rated current. (a) Increasing power. (b) Decreasing power.

two curves of typical rate of change of normalized LED current $I_{\text{LED\_norm}}$ are obtained and shown in Fig. 7. It can be observed that the typical curves for increasing and decreasing current are symmetrical. In Fig. 7(a), the rate of change of LED current above the typical curve means the power change and light variation could significantly affect the human vision. On the contrary, the rate of change of LED current below the typical curve means a minor effect and smooth change of light intensity which is acceptable to the majority of the interviewees. It is important to note that the typical curve is comprised of three segments with different percentages of rated LED current. In the low-power range from 15% to 33% of rated LED current, 6.4 s is needed to increase the LED current. The rate of change of current is only about 2.8% per second. In the medium power range from 33% to 50%, the time required is shortened to 2.8 s. The rate of change of current has increased to 6.1% per second. The current over 50% of the rated current is classified into high-power range. In this range, the rate of change of current is substantially increased to 15% per second. The rate of change of LED current in high-power range can be much faster than low-power range. This result well agrees with Fig. 4 that human eye perceives light in a logarithmic manner. The results obtained in Fig. 7 will be further incorporated into the controller design of the proposed smart LED driver.

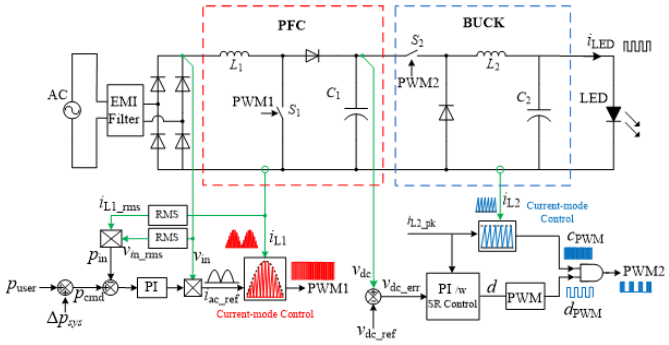

Fig. 8. Simplified schematic of the proposed smart LED driver.

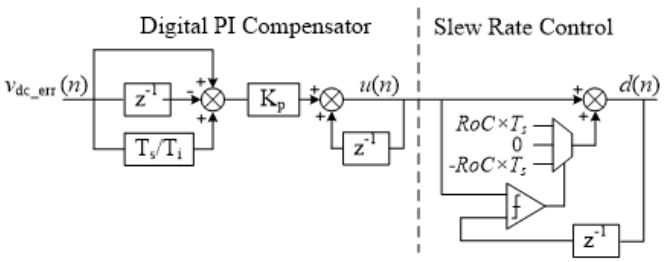

Fig. 9. Digital implementation of PI compensator and slew rate control.

IV. Prototyping and Control Implementation

A simplified schematic of the proposed smart LED driver is depicted in Fig. 8. At the input side, a boost converter is used to provide PFC. At the output side, a buck converter is used to control the LED current.

A. PFC Converter

In the PFC converter, the conventional output dc voltage control loop is replaced by an input power control loop to generate the current reference $i_{\text{ac\_ref}}$ as shown in Fig. 8. The input power command p_{cmd} is comprised of two parts: p_{user} is the brightness control from user and Δp_{sys} is the power command from power system operator. The error between p_{cmd} and measured input power p_{in} is applied to a PI compensator to generate the current reference $i_{\text{ac\_ref}}$. $i_{\text{ac\_ref}}$ and the inductor current i_{L1} are fed to the current-mode controller to produce a pulsewidth modulation (PWM) signal PWM1 for the switch S_1. The PFC is operated in the boundary conduction mode shaping the input current to follow the sinusoidal ac voltage.

B. DC/DC Converter

The dc/dc converter is a buck converter controlling the LED current i_{LED} and the dc voltage v_{dc} across C_1.To regulate the LED current, the measured inductor current i_{L2} is fed to a current-mode controller to produce a PWM signal c_{PWM}. The peak of i_{L2} is controlled at a constant value $I_{\text{L2\_pk}}$, and the magnitude of the LED current is equal to $I_{\text{L2\_pk}}/2$. Then, c_{PWM} is further modulated by d_{PWM} to change the average current and power of the LED to regulate the dc voltage v_{dc}.

Note that the rate of change of LED current should be controlled properly in order to reduce the visual discomfort for human eye. Therefore, the response time of the dc/dc converter is slower than the PFC converter. The power mismatch between two converters leads to generate voltage fluctuation in v_{dc}. The error between the measured dc voltage v_{dc} and the reference $v_{\text{dc\_ref}}$ is applied to a PI compensator to generate the control command d. The slew rate of the PI compensator is designed to follow a typical rate of change of LED current. Fig. 9 shows the signal flow diagram of a digital PI compensator with slew rate control. The transfer function of the PI compensator in discrete form is expressed as

$$u(n) = u(n-1) + K_p[V_{\text{dc\_err}}(n) - V_{\text{dc\_err}}(n-1)] + K_{\text{p}}\frac{T_s}{T_i}V_{\text{dc\_err}}(n) \quad (11)$$

where $u(n)$, $u(n-1)$ and $v_{\text{dc\_err}}(n)$, $v_{\text{dc\_err}}(n-1)$ are the output values and input errors of PI compensator at the present and past samplings, respectively. K_{p} is the proportional gain constant. T_{i} and T_{s} are the integral time constant and sampling time of the controller, respectively. In the section of slew rate control, the present $u(n)$ is compared with the past $d(n-1)$ to control the slew rate of $d(n)$. The transfer function to represent the relationship of $u(n)$, $d(n)$, and slew rate is formulated as

$$d(n) = \begin{cases} u(n) + \text{RoC} \times T_s, & u(n) > d(n-1) \\ u(n), & u(n) = d(n-1) \\ u(n) - \text{RoC} \times T_s, & u(n) < d(n-1). \end{cases} \quad (12)$$

The typical RoC provides a well balance between high visual comfort and low voltage variation of v_{dc}. A PWM generator is used to convert $d(n)$ into a PWM signal d_{PWM}.

Note that the frequency of d_{PWM} must be faster than the human eye can detect to avoid flickering effects (i.e., >200 Hz). The average current of the LED I_{LED} becomes proportional to the duty cycle of d_{PWM}. It can be expressed as $I_{\text{LED}} = d \times ((I_{\text{L2\_pk}})/2)$, where d is the duty cycle of the d_{PWM}. The power of the LED is changed proportionally with the average current.

V. Practical Implementation and Results

A. Hardware

An experimental hardware is built by modifying a commercially available LED driver UCC28810EVM-002 from Texas Instruments [27]. The original discrete control circuit is disabled and the new control method is implemented in a TMS320F28069 digital signal processor. Fig. 10 shows a photograph of the prototype. An LED lamp from Philips (Fortimo LED DLM, Module 2000 32 W/840) is driven by the proposed smart LED driver. The parameters of the smart LED driver are listed in Table II. The LED driver is tested under two different input functions. Measured waveforms of the input power p_{in}, dc voltage v_{dc}, control signal d, and brightness of LED are recorded. Fig. 11 shows a ramp input function changing from 26 to 30 W in 2 s. The control signal d changes from 0.75 to 0.88 and the brightness of LED changes from 467 to 548 lux accordingly. Since the rate of change of

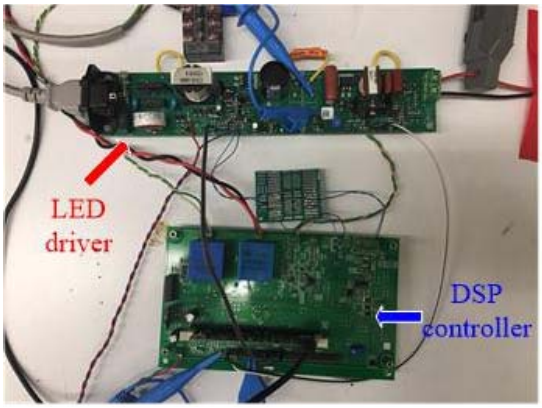

Fig. 10. Experimental hardware.

TABLE II
PARAMETERS OF THE SMART LED DRIVER

Parameters	*Values*
PFC Inductor L_1	*1mH*
BUCK Inductor L_2	*400μH*
DC Capacitor C_1	*82μF*
Buck Output Capacitor C_2	*2.5μF*

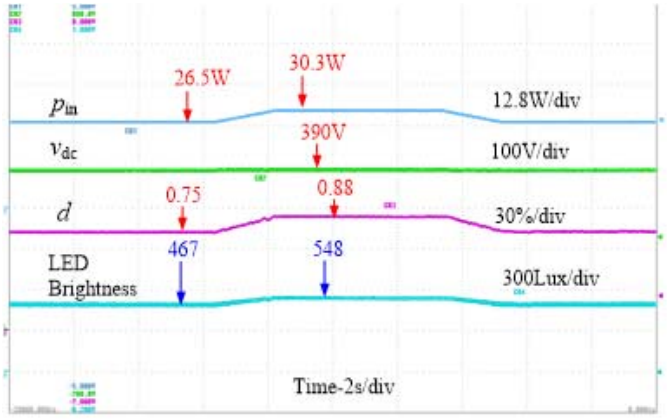

Fig. 11. Waveforms of the proposed smart LED driver under a ramp input function.

the input power is small, the brightness of the LED follows the input power. It can be observed that v_{dc} is regulated at 390 V.

The measured waveforms of the proposed LED driver responding to a step input function are shown in Fig. 12. In this example, the PFC converter receives the power command to increase the power consumption from 26 to 30 W immediately. The dc voltage v_{dc} rises up due to excess input power. The PI compensator in the dc/dc converter responses to the rise of v_{dc}, and thus, d gradually increases. It can be observed that d does not follow the step input function. Instead, it rises slowly following the typical rate of change of LED current. The power of the LED keeps increasing slowly until the dc voltage drops below the reference value. Thus, a negative error is generated and the PI compensator reduces d to eliminate steady-state error. Similarly, in the case of load shedding, a decline in the dc voltage generates a negative error to the PI compensator.

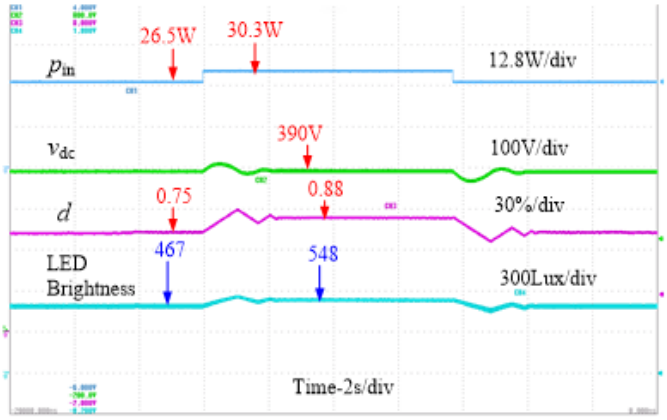

Fig. 12. Waveforms of the proposed smart LED driver under a step input function.

d gradually decreases, as a result, the power of the LED reduces. The rate of decline of d is controlled following the typical RoC of LED current. The output power of the PFC and input power of the dc/dc converter are equal when the steady-state condition is reached.

B. Evaluation With Interviewees

Visual assessments are conducted to evaluate the performance of the proposed control method. The 17 interviewees from 23 to 40 years of age are invited to participate in the visual assessments. Each of the assessment takes 200 s. The interviewees are invited to read an article in the light chamber. They are instructed to press a switch button when they notice the change of light intensity during the assessment. The variation of the input power p_{in}, dc voltage v_{dc}, control signal d, brightness of the LED, and trigger pulse generated by the switch button is recorded.

To emulate a mild power fluctuation in the power distribution network, a prerecorded ramp input function of 200 s is fed to the smart LED driver. The slew rate control circuit of the smart LED driver is deactivated in the first assessment. The test result of one of the interviewees is shown in Fig. 13(a). d and brightness of the LED follow the fairly slow rate of change of input power. The power profile consists of 19 changing points. Six trigger pulses are occasionally recorded during the assessment. This indicates that a slow variation of LED power does not have a huge amount of influence to the interviewee. Afterward, the same 200-s power profile is repeated with the slew rate control of the smart LED driver is activated. Fig. 13(b) shows the measurement result of the same interviewee in the second assessment. Since both the input power and LED power change mildly, the power difference between the input and LED is very small. The voltage variation in v_{dc} is insignificant. Detailed waveforms are provided in Fig. 13(c) to show the difference with and without slew rate control. However, it can be seen that the number of trigger pulses has been reduced to four when the slew rate control is activated.

Since the wind and solar energy varies all the time, the power system operator needs to react to the rapid change of power generation from these renewable energy sources.

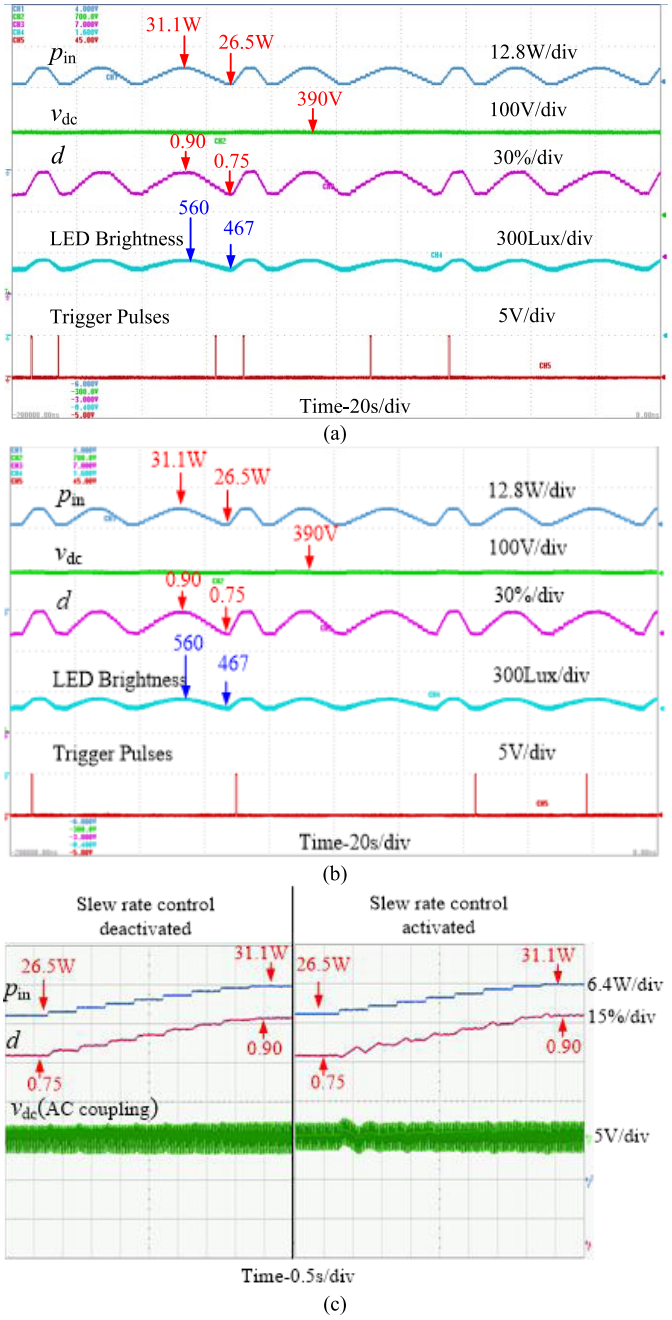

Fig. 13. Measurement results of the visual assessments with slow ramp input power profile. (a) First assessment with the slew rate control deactivated. (b) Second assessment with the slew rate control activated. (c) Detailed waveforms of p_{in}, d, and v_{dc} of the first and second assessments during 70–75 s.

A prerecorded step input function of 200 s is fed to the smart LED driver to emulate a rapid power change in the power distribution network. Fig. 14(a) shows the captured waveforms of the third assessment with the slew rate control deactivated. It can be seen that d follows p_{in} and v_{dc} is tightly regulated at a constant value.

The step input function consists of 40 changing points. It can be observed that the light flicking due to rapid change of LED power is noticed by the interviewee. The 33 trigger pulses are recorded. The trigger pulses are frequently generated when

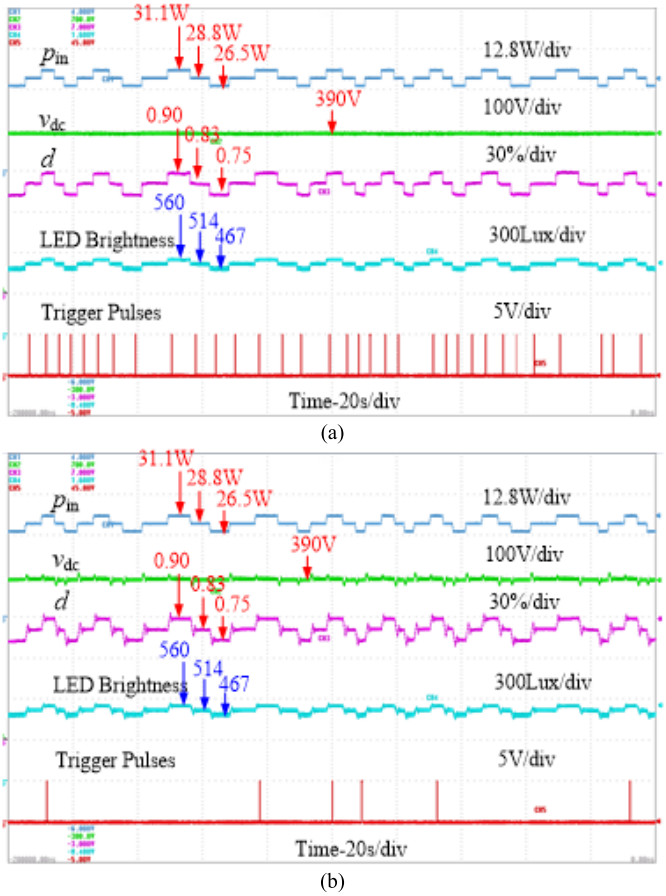

Fig. 14. Measurement results of visual assessment with step input function. (a) Third assessment with the slew rate control deactivated. (b) Fourth assessment with the slew rate control activated.

the LED driver changes the power to follow the input power command. The same step input function is repeated with the slew rate control activated in the fourth assessment. The results are shown in Fig. 14(b). With the slew rate control activated, the LED power does not follow the change of input power. Instead, the change of LED power is controlled to follow a typical RoC. The fluctuation of v_{dc} due to the power imbalance between the PFC and dc/dc converters can be clearly observed. C_1 acts as a temporary storage to absorb the power fluctuation. Since the rate of change of LED power has been reduced, a number of trigger pulses have substantially reduced. Only six pulses are recorded which is five times less than without slew rate control in the third assessment. This implies that the slew rate control in the smart LED driver could substantially reduce the light flickering and enhance the visual comfort to the user.

The same assessments are conducted on 17 interviewees. The average numbers of trigger pulses recorded in four assessments are shown in Fig. 15. Without the slew rate control activated, the first assessment with ramp input function shows seven trigger pulses, which is acceptable to the most of interviewees. Nevertheless, it is rated the highest number of trigger pulses by the interviewees in the third visual assessment with step input function. The two results agree with the scientific study that human eye is sensitive to rapid

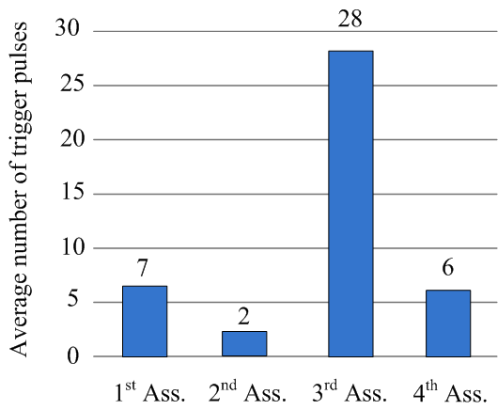

Fig. 15. Average number of trigger pulses of the visual assessments. (Note: First assessment—ramp input function with slew rate control deactivated. Second assessment—ramp input function with slew rate control activated. Third assessment—step input function with slew rate control deactivated. Fourth assessment—step input function with slew rate control activated.)

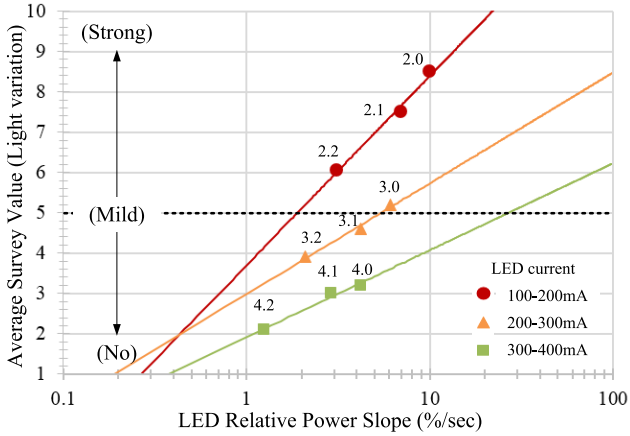

Fig. 16. Extrapolation of the LED brightness visual perception experiment "How extreme do you notice the light variation?"

light variation. While the same step input function is used in the fourth assessment, the number of trigger pulses remains as low as the first assessment with ramp input function and slew rate control deactivated. In the second assessment with ramp input function, the slew rate control also significantly reduces the average number of trigger pulses from 7 to 2. It can be seen that the proposed new control method performs very well in responding to the change of input power. The change of LED power is controlled to follow the typical RoC to avoid light annoyance to the user. Note that the high sensitivity of human eye to rapid change of ambient light intensity was an obstacle to implement the demand response control in the lighting system. Using the same power converter circuit, we demonstrated the visual comfort can be greatly improved by properly designed control method. This new proposal opens a new control dimension in the smart grid with high penetration of renewable energy. Lighting system becomes a key member of electric appliances to provide automatic demand response. They can play a significant role to balance system load and increase the reliability of the electricity grid.

VI. Conclusion

Different from the traditional LED driver control method, a new power control method with the consideration of human visual perception is presented in this paper. This paper starts by conducting a series of visual assessments to investigate the human eye response to the change of light intensity. The results agree with the scientific reports that human eye perceives light in a logarithmic manner. It is, therefore, the variation of light intensity in low light level is easier to be noticed than in high light level. Based on this conclusion, the typical rate of change of LED power curves is constructed through the collected data. A slew rate control is implemented in the LED driver to limit the rate of change of LED power. An experimental hardware is built to evaluate the effectiveness of the proposed control method to eliminate the disruption to the human. The results indicate that the proposed control method scan effectively alleviates the LED light fluctuation under various input functions. This paper demonstrates the concept of smart lighting systems as a demand response solution to the future power grid with substantial penetration of intermittent renewable energy sources.

Appendix

Fig. 16 summarizes the most important results of the survey to find out how extreme do people notice the light variation. The horizontal axis relates to the relative ramp rate applied to the LED during the experiments. The power rate is related to the average power of the lamp during the performing of the test. Since we anticipate that humans perceive light in a logarithmic manner (as explained previously), the axis is also scaled logarithmically. On the vertical axis, the average survey value relating to the presented ramp rates is given. The upper three points are related to the experimental data with a high brightness level, the ones in the middle to a medium brightness level, and the three lower points to a low light level. Extrapolating the lines to a survey value of "1" should result in a ramp rate, which will not be perceived at all. As an average, a ramp rate of 0.3% results, which can be considered as the perception limit. However, a higher ramp rate can be considered in practical applications: using a ramp rate leading to an average survey value of 5 can be considered as a mild variation. Such ramp rates were used in the prototype for the visual assessments.

References

[1] Eurostat Press Office. (2017). *Eleven EU Countries Hit 2020 Renewable Energy Targets*. [Online]. Available: http://ec.europa.eu/energy/en/news/eleven-eu-countries-hit-2020-renewable-energy-targets

[2] B. Kroposki *et al.*, "Achieving a 100% renewable grid: Operating electric power systems with extremely high levels of variable renewable energy," *IEEE Power Energy Mag.*, vol. 15, no. 2, pp. 61–73, Mar./Apr. 2017.

[3] M. Milligan *et al.*, "Alternatives no more: Wind and solar power are mainstays of a clean, reliable, affordable grid," *IEEE Power Energy Mag.*, vol. 13, no. 6, pp. 78–87, Nov./Dec. 2015.

[4] E. J. Coster, J. M. A. Myrzik, B. Kruimer, and W. L. Kling, "Integration issues of distributed generation in distribution grids," *Proc. IEEE*, vol. 99, no. 1, pp. 28–39, Jan. 2011.

[5] P. Kundur, *Power System Stability and Control*. New York, NY, USA: McGraw-Hill, 1994.

[6] N. G. Hingorani and L. Gyugyi, *Understanding FACTS: Concepts and Technology of Flexible AC Transmission Systems*. Hoboken, NJ, USA: Wiley, 2000.

[7] M. Bragard *et al.*, "The balance of renewable sources and user demands in grids: Power electronics for modular battery energy storage systems," *IEEE Trans. Power Electron.*, vol. 25, no. 12, pp. 3049–3056, Dec. 2010.

[8] S. D. G. Jayasinghe, D. M. Vilathgamuwa, and U. K. Madawala, "Diode-clamped three-level inverter-based battery/supercapacitor direct integration scheme for renewable energy systems," *IEEE Trans. Power Electron.*, vol. 26, no. 12, pp. 3720–3729, Dec. 2011.

[9] P. Palensky and D. Dietrich, "Demand side management: Demand response, intelligent energy systems, and smart loads," *IEEE Trans. Ind. Informat.*, vol. 7, no. 3, pp. 381–388, Aug. 2011.

[10] J. A. Short, D. G. Infield, and L. L. Freris, "Stabilization of grid frequency through dynamic demand control," *IEEE Trans. Power Syst.*, vol. 22, no. 3, pp. 1284–1293, Aug. 2007.

[11] Z. Chen, L. Wu, and Y. Fu, "Real-time price-based demand response management for residential appliances via stochastic optimization and robust optimization," *IEEE Trans. Smart Grid*, vol. 3, no. 4, pp. 1822–1831, Dec. 2012.

[12] S. Y. Hui, C. K. Lee, and F. F. Wu, "Electric springs—A new smart grid technology," *IEEE Trans. Smart Grid*, vol. 3, no. 3, pp. 1552–1561, Sep. 2012.

[13] C. K. Lee, B. Chaudhuri, and S. Y. Hui, "Hardware and control implementation of electric springs for stabilizing future smart grid with intermittent renewable energy sources," *IEEE J. Emerg. Sel. Topics Power Electron.*, vol. 1, no. 1, pp. 18–27, Mar. 2013.

[14] Z. Akhtar, B. Chaudhuri, and S. Y. R. Hui, "Smart loads for voltage control in distribution networks," *IEEE Trans. Smart Grid*, vol. 8, no. 2, pp. 937–946, Mar. 2017.

[15] V. Trovato, I. M. Sanz, B. Chaudhuri, and G. Strbac, "Advanced control of thermostatic loads for rapid frequency response in Great Britain," *IEEE Trans. Power Syst.*, vol. 32, no. 3, pp. 2106–2117, May 2017.

[16] X. Luo, C. K. Lee, W. M. Ng, S. Yan, B. Chaudhuri, and S. Y. R. Hui, "Use of adaptive thermal storage system as smart load for voltage control and demand response," *IEEE Trans. Smart Grid*, vol. 8, no. 3, pp. 1231–1241, May 2017.

[17] C. K. Lee, S. Li, and S. Y. Hui, "A design methodology for smart LED lighting systems powered by weakly regulated renewable power grids," *IEEE Trans. Smart Grid*, vol. 2, no. 3, pp. 548–554, Sep. 2011.

[18] Q. Wang, M. Cheng, and B. Zhang, "An improved topology for the current fed parallel resonant half bridge circuits used in fluorescent lamp electronic ballasts," *J. Power Electron.*, vol. 15, no. 2, pp. 567–575, Mar. 2015.

[19] O. Hafez and K. Bhattacharya, "Integrating EV charging stations as smart loads for demand response provisions in distribution systems," *IEEE Trans. Smart Grid*, vol. 9, no. 2, pp. 1096–1106, Mar. 2018.

[20] X. Zhou, Y. Ma, Z. Gao, and H. Wang, "Summary of smart metering and smart grid communication," in *Proc. IEEE Int. Conf. Mechatronics Automat. (ICMA)*, Aug. 2017, pp. 300–304.

[21] C. Zhao, J. He, P. Cheng, and J. Chen, "Consensus-based energy management in smart grid with transmission losses and directed communication," *IEEE Trans. Smart Grid*, vol. 8, no. 5, pp. 2049–2061, Sep. 2017.

[22] EMSD. (2018). *Hong Kong Energy End-Use Data 2018*. [Online]. Available: https://www.emsd.gov.hk/filemanager/en/content_762/HKEEUD2018.pdf

[23] R. Budzilek. (2016). *Linear vs. Logarithmic Dimming*. [Online]. Available: http://pathwaylighting.com/blogposts/details/44

[24] E. Waffenschmidt, A. Kores, D. Fuh, L. C. Kwan, and L. Heng, "Grid control with led lamps," in *Proc. 7th Int. Energy Sustain. Conf. (IESC)*, May 2018, pp. 1–7.

[25] P. Boyce and P. Raynham, *LH SLL Lighting Handbook*. London, U.K.: The Chartered Institution of Building Services Engineers, 2018.

[26] D. L. Dilaura *et al.*, *Lighting Handbook: Reference Application*, 8th ed. New York, NY, USA: Illuminating Engineering, 1993.

[27] *Using the UCC28810EVM-002 User's Guide*. Accessed: Jun. 2009. [Online]. Available: http://www.ti.com/lit/ug/sluu355a/sluu355a.pdf

Chi Kwan Lee (M'08–SM'14) received the B.Eng. and Ph.D. degrees in electronic engineering from the City University of Hong Kong, Hong Kong, in 1999 and 2004, respectively.

From 2004 to 2005, he was a Post-Doctoral Research Fellow with the Power and Energy Research Center, National University of Ireland, Galway, Ireland. In 2006, he joined the Center of Power Electronics, City University of Hong Kong, as a Research Fellow. From 2008 to 2011, he was a Lecturer of electrical engineering with the Hong Kong Polytechnic University, Hong Kong. Since 2010, he has been a Visiting Researcher with the Imperial College London, London, U.K. He is currently an Associate Professor with the Department of Electrical and Electronic Engineering, The University of Hong Kong, Hong Kong. He is a Co-Inventor of the Electric Springs and Planar Electromagnetic Interference Filter. His current research interests include wireless power transfer, clean energy technologies, and smart grids.

Dr. Lee was a recipient of the IEEE Power Electronics Transactions First Prize Paper Award for his publications on Mid-Range Wireless Power Transfer in 2015.

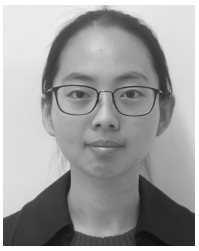

Heng Liu received the B.Eng. and M.Phil. degrees in electrical engineering from Zhejiang University, Hangzhou, China, in 2011 and 2014, respectively. She is currently pursuing the Ph.D. degree with the Department of Electrical and Electronic Engineering, The University of Hong Kong, Hong Kong.

Her current research interests include smart grid and power electronic technologies.

Desiree Fuhs was born in Dormagen, Germany, in 1990. She received the Technical Diploma degree in electronics from the Berufskolleg für Technik und Informatik (workers college for technology and computer science), Neuss, Germany, in 2010, the B.Eng. degree in electrical engineering with the field of drive and automation technology from the University of Applied Science, Aachen, Germany, in 2014, and the M.Sc. degree in the field of renewable energies from the University of Technology, Arts and Science, Cologne, Germany, in 2018.

She was in an apprenticeship as an Electronics Engineer of industrial engineering in 2007 and became a craftsman in this field in 2010 at Hydro Aluminium Neuss GmbH & Co., KG, Neuss. She is currently a Project Engineer in consulting and engineering of innovative projects at paXos Consulting & Engineering GmbH & Co., KG, Cologne.

André Kores received the B.Eng. and M.Sc. degrees in renewable energies from the Cologne University of Applied Sciences, Cologne, Germany, in 2016 and 2018, respectively.

Eberhard Waffenschmidt (M'04–SM'10) received the Dr.Ing. degree in electronic engineering and the Ph.D. degree from RWTH Technical University, Aachen, Germany.

From 1995 to 2011, he was with Philips Research, Aachen, finally as a Senior Scientist. Since 2011, he has been a Professor of electrical power grids with the TH Köln—University of Applied Sciences, Cologne, Germany. He is currently the Chairman of the Solarenergie-Förderverein Deutschland e.V. (SFV, Society to Promote Solar Energy Germany), Aachen. His current research interests include identifying and removing obstacles on the way to a 100% use of renewable energy.